Front. Mater. Sci. 2017, 11(2): 182–189
DOI 10.1007/s11706-017-0376-x

RESEARCH ARTICLE

# Electronic structure and bonding interactions in $Ba_{1-x}Sr_xZr_{0.1}Ti_{0.9}O_3$ ceramics

Jegannathan MANGAIYARKKARASI (✉)[1], Subramanian SASIKUMAR[2], Olai Vasu SARAVANAN[2], and Ramachandran SARAVANAN[2]

1 PG and Research Department of Physics, NMSSVN College, Nagamalai, Madurai-625 019, Tamil Nadu, India
2 Research Centre and PG Department of Physics, The Madura College, Madurai-625 011, Tamil Nadu, India

© Higher Education Press and Springer-Verlag Berlin Heidelberg 2017

**ABSTRACT: An investigation on the precise electronic structure and bonding interactions has been carried out on $Ba_{1-x}Sr_xZr_{0.1}Ti_{0.9}O_3$ (short for BSZT, $x$ = 0, 0.05, 0.07 and 0.14) ceramic systems prepared via high-temperature solid state reaction technique. The influence of Sr doping on the BSZT structure has been examined by characterizing the prepared samples using PXRD, UV-visible spectrophotometry, SEM and EDS. Powder profile refinement of X-ray data confirms that all the synthesized samples have been crystallized in cubic perovskite structure with single phase. Charge density distribution of the BSZT systems has been completely analyzed by the maximum entropy method (MEM). Co-substitution of Sr at the Ba site and Zr at the Ti site into the $BaTiO_3$ structure presents the ionic nature between Ba and O ions and the covalent nature between Ti and O ions, revealed from MEM calculations. Optical band gap values have been evaluated from UV-visible absorption spectra. Particles with irregular shapes and well defined grain boundaries are clearly visualized from SEM images. The phase purity of the prepared samples is further confirmed by EDS qualitative spectral analysis.**

**KEYWORDS: barium titanate; X-ray diffraction; Rietveld refinement; maximum entropy method; bonding**

## Contents



Received December 29, 2016; accepted March 13, 2017

E-mail: mangai.jp@gmail.com

## 1 Introduction

Recently, perovskite-based titanate oxides $BaTiO_3$ have attracted huge attention due to their wide spread applications in the field of electronics and communications [1]. Substitution of selected dopant ions plays a significant role in improving the essential properties of barium titanate [2]. Particularly, $Zr^{4+}$ substitution at the $Ti^{4+}$ site has been reported as an effective way to decrease the Curie

temperature [3]. $BaZr_xTi_{1-x}O_3$ ceramic systems are known to be the promising materials for dielectrics in commercial capacitors and also in dynamic random access memory (DRAM) and micro electro-mechanical systems (MEMS) [4–5]. The BZT ceramic materials are widely accepted as the favorable materials for piezoelectric sensors and actuators [6]. In the form of thin films, Zr-doped $BaTiO_3$ (BZT) materials exhibit interesting optical properties like complex refractive index, IR responses and photoluminescence [7]. It has been reported that Sr-substituted $BaTiO_3$ solid solutions could be used in numerous applications, for example in tunable filters, microwave phase shifters, multilayer ceramic capacitors (MLCCs) and oscillators [8–9]. Dielectric resonators and GPS antennas made up of Sr-doped $BaTiO_3$ (BST) materials have become attractive due to the zero conductor loss and better gain efficiency compared to other materials [10]. BST materials are also largely used in electro-optic devices and pyroelectric detectors. The huge number of applications of BST and BZT prompted the authors to investigate the Sr and Zr co-substitutional effects on the structural and charge derived properties of $Ba_{1-x}Sr_xZr_{0.1}Ti_{0.9}O_3$ (BSZT) ceramics [11]. Simultaneous addition of Sr and Zr into the $BaTiO_3$ structure is an effective strategy to preserve and to substantially enhance the desirable properties [12]. Substitutions of Sr at the lattice site of Ba and Zr at the lattice site of Ti in $BaTiO_3$ consequently set down the Curie temperature ($T_C$), and enhance the dielectric constant of the material near room temperature [13]. In this work, $BaZr_{0.1}Ti_{0.9}O_3$ composition was chosen as the basic solid solution for the addition of Sr, because it was reported that among the $BaZr_xTi_{1-x}O_3$ series, $BaZr_{0.1}Ti_{0.9}O_3$ has shown the superior dielectric and ferroelectric properties [14]. Preparations through chemical methods and sol–gel process produce non-uniform grains and also suppressed the value of dielectric constant whereas the high-temperature solid state method ensures stabilizing the metastable phases and eliminating the intermediate additional phases [15]. In the present work, all the samples of BSZT have been prepared via high-temperature solid state reaction method to get phase pure samples.

A few researchers have reported the experimental analysis on the structural and dielectric properties of the BSZT systems [16–17] but the studies on precise electronic structure and bonding are lacking in literatures. The electronic structure of undoped $BaTiO_3$ has been investigated theoretically by Deng et al. [18]. The detailed investigation of the internal electronic structure, electron density re-distributions and bonding between the constituent atoms in the prepared systems is very much essential to select a material for specific device applications [19]. So this work has mainly been focused towards the charge related properties and bonding interactions, especially around Ba – O and Ti – O bonds in the unit cell of BSZT ceramic systems. In the present analysis, powder X-ray data have been subjected to the Rietveld refinement [20] and the structure factors extracted from the refinement have been utilized for the maximum entropy method (MEM) [21] to elucidate the precise electron density distributions. The inter-atomic bonding nature between the Ba – O and Ti – O bonds have been discussed properly by analyzing 3D, 2D and 1D electron density distribution in the BSZT ceramics. The structural characterization, optical properties, surface morphology and the chemical compositions of the synthesized samples were also investigated through powder X-ray diffraction (PXRD), UV-visible absorption spectrometry (UV-vis), scanning electron microscopy (SEM) and energy dispersive X-ray spectroscopy (EDS), respectively.

## 2 Experimental

### 2.1 Synthesis of $Ba_{1-x}Sr_xZr_{0.1}Ti_{0.9}O_3$ ceramics

$Ba_{1-x}Sr_xZr_{0.1}Ti_{0.9}O_3$ ceramics with various compositions of $x$ = 0, 0.05, 0.07 and 0.14 have been prepared by the solid state reaction technique using the high-purity starting materials (Alfa Aesar, 99.99%). Stoichiometric amounts of $BaCO_3$, $SrCO_3$, $ZrO_2$ and $TiO_2$ were thoroughly ground using an agate mortar and then calcined at 1250ºC for 15 h in alumina crucibles using a tubular furnace. During the synthesis, a chemical reaction takes place as follows:

$$(1-x)BaCO_3 + xSrCO_3 + 0.1ZrO_2 + 0.9TiO_2 \rightarrow Ba_{1-x}Sr_xZr_{0.1}Ti_{0.9}O_3 + CO_2 \uparrow \quad (1)$$

After calcination, the powder compounds were again ground using an agate mortar and compressed into dense pellets by applying the uni-axial pressure of 6 tons. These pellets were finally sintered at a high temperature of 1500ºC for 8 h at a programmed heating rate of 5ºC/min in air atmosphere. Then, the sintered samples were furnace cooled to room temperature and crushed as fine powder for further characterization studies. Figure 1 shows the synthesized $Ba_{1-x}Sr_xZr_{0.1}Ti_{0.9}O_3$ ($x$ = 0, 0.05, 0.07 and 0.14) samples.

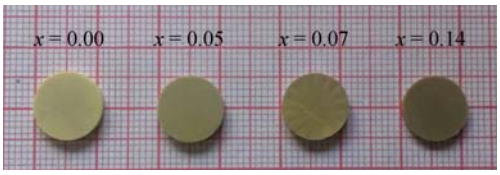


**Fig. 1** $Ba_{1-x}Sr_xZr_{0.1}Ti_{0.9}O_3$ samples synthesized by the solid state reaction method.

### 2.2 Characterizations

PXRD patterns of the prepared BSZT samples were recorded at room temperature using Bruker AXS D8 advance X-ray diffractometer with Cu Kα monochromatic incident radiation ($\lambda$ = 1.54056 Å), with the step scan of 0.02º, in the $2\theta$ range of 10º–120º, collected at Sophisticated Analytical Instrument Facility (SAIF), Cochin University, Cochin, India. The optical absorption spectra were recorded in the wavelength range of 200–2000 nm using UV-vis spectrophotometer (Cary 5000, Varian, Germany). Microstructures of the samples were analyzed using scanning electron microscope (Carl Zeiss Evo 18) and elemental compositions of the samples were checked using energy dispersive X-ray spectrometer (Quantax 200 with X-flash-Bruker) collected at International Research Centre, Kalasalingam University, Krishnankoil, Tamil Nadu, India.

## 3 Results and discussion

### 3.1 XRD analysis

Structural characterizations have been carried out using powder X-ray data. Figure 2(a) shows the raw X-ray profiles of the samples for various Sr concentrations. Figure 2(b) shows the enlarged XRD peak corresponding to the (220) plane, which clearly demonstrates the peak shifting towards higher $2\theta$ angle. The shifting of Bragg peaks indicates the decrease in cell parameter due to the doping of smaller $Sr^{2+}$ (ionic radius 1.13 Å) at the lattice site of larger $Ba^{2+}$ (ionic radius 1.35 Å) [22]. The peak shift qualitatively confirms that, Sr is systematically well substituted in the chosen compositional range.

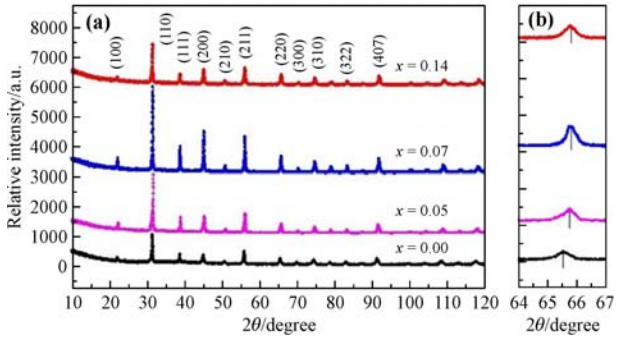


**Fig. 2** **(a)** Observed PXRD patterns of $Ba_{1-x}Sr_xZr_{0.1}Ti_{0.9}O_3$ with $x$ = 0, 0.05, 0.07 and 0.14. **(b)** Enlarged XRD peaks of the (220) plane.

### 3.2 Powder profile refinement

The phase formations of the prepared BSZT samples have been analyzed by comparing the experimental XRD profiles with the JCPDS (Joint Committee on Powder Diffraction Standards). All the Bragg peaks have been matched well with the powder diffraction file number 31-0174 which confirms that all the prepared BSZT systems have been well crystallized in perovskite cubic structure. No other additional peaks are detected from the XRD patterns which clearly indicate the single phase formation of the prepared ceramic systems. The detailed structural studies of the BSZT samples were carried out by refining the experimentally observed powder profiles using Rietveld refinement [20] with software JANA 2006 [23]. In the prepared series of BSZT solid solutions with the $ABO_3$ perovskite structure, Ba and Sr ions are occupying A-site while Ti and Zr ions are occupying B-site. The XRD profiles of BSZT were refined by considering the cubic setting with space group $Pm\bar{3}\,m$ (space group number: 221) and one formula unit per unit cell. In the cubic setting, Ba and Sr atoms are fixed at (0, 0, 0), Ti and Zr atoms are fixed at (0.5, 0.5, 0.5) and oxygen is at (0.5, 0.5, 0) positions given by Wyckoff [24]. The refined profiles of $Ba_{1-x}Sr_xZr_{0.1}Ti_{0.9}O_3$ ($x$ = 0, 0.05, 0.07 and 0.14) are given in Figs. 3(a)–3(d). In these figures, the observed profiles and calculated profiles are indicated by cross marks and continuous lines, respectively. The positions of the Bragg peaks are denoted by the vertical lines. The difference between the observed and calculated profiles is given at the bottom of each figure. The fitted profiles reveal the good matching between the observed and calculated profiles for all the four compositions. The refined structural parameters, $R_p$, $R_{obs}$ and GOF (goodness of fit) values are presented in Table 1. The decrease in cell parameters and the shrinkage in cell volume with Sr concentrations are due to the substitution of smaller $Sr^{2+}$ (ionic radius: 1.13 Å) at the lattice sites of $Ba^{2+}$ (ionic radius: 1.35 Å) [22]. The calculated lattice parameters are in agreement with the reported values [25].

The average crystallite sizes of the synthesized BSZT

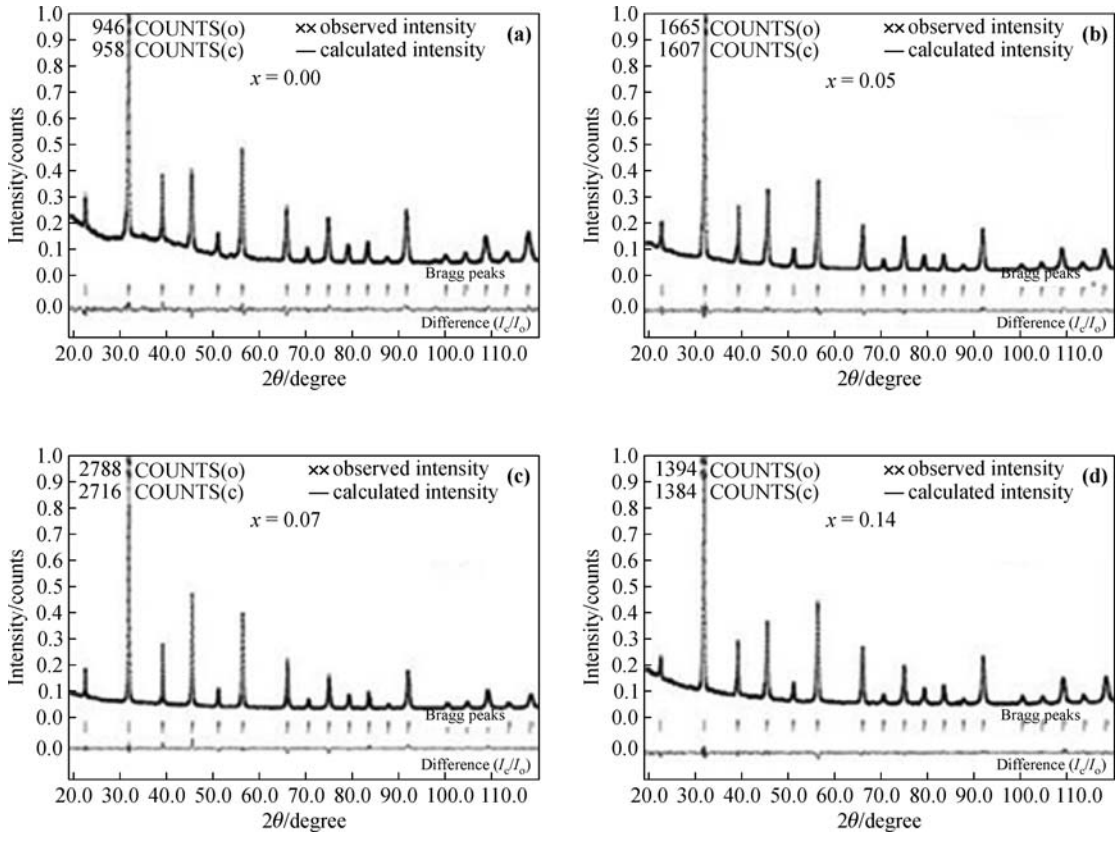


**Fig. 3** Fitted PXRD profiles for $Ba_{1-x}Sr_xZr_{0.1}Ti_{0.9}O_3$: **(a)** $x$ = 0; **(b)** $x$ = 0.05; **(c)** $x$ = 0.07; **(d)** $x$ = 0.14.

**Table 1** Refined parameters of $Ba_{1-x}Sr_xZr_{0.1}Ti_{0.9}O_3$ with $x$ = 0, 0.05, 0.07 and 0.14 through refinement of powder XRD data

| Sample | Parameters | | | | | | | |
|---|---|---|---|---|---|---|---|---|
| | $a=b=c$ /Å | $\alpha=\beta=\gamma$ /(°) | Volume /Å$^3$ | Density /(g·cm$^{-3}$) | $R_p$ /% | $R_{obs}$ /% | GOF | $F_{(000)}$ |
| $x$ = 0.00 | 4.0313(8) | 90 | 65.43(1) | 6.02(2) | 3.39 | 2.53 | 0.48 | 104 |
| $x$ = 0.05 | 4.0257(9) | 90 | 65.22(1) | 5.98(1) | 8.32 | 2.14 | 1.15 | 103 |
| $x$ = 0.07 | 4.0120(2) | 90 | 64.57(2) | 6.02(2) | 7.14 | 2.99 | 1.10 | 103 |
| $x$ = 0.14 | 4.0054(6) | 90 | 64.12(3) | 5.96(2) | 8.09 | 4.17 | 1.11 | 101 |

Notes: $R_p$, profile reliability factor; $R_{obs}$, observed profile reliability factor; GOF, goodness of fit; $F_{(000)}$, number of electrons in the unit cell.

samples have been calculated through GRAIN software [26] using the Scherrer formula:

$$t = \frac{0.9\lambda}{\beta\cos\theta} \tag{2}$$

where $t$ is the average crystallite size of the coherently diffracting domains, $\theta$ is the Bragg angle, $\beta$ is the full width at half maximum (FWHM), and $\lambda$ is the wavelength of X-ray (1.54056 Å). The average crystallite sizes of the synthesized samples are calculated in the range of 21–32 nm.

### 3.3 Charge density distribution and bonding interactions

The electronic structure, charge density distribution and the bonding interactions of the $Ba_{1-x}Sr_xZr_{0.1}Ti_{0.9}O_3$ systems have been analyzed by the MEM [21] using the structure factors obtained from the Rietveld refinement [20]. The MEM [21] calculations were carried out successfully by implementing the software PRIMA [27], considering 64×64×64 pixels per cubic unit cell. The resultant 3D charge density distribution and 2D contour maps were plotted with similar iso-surface level of 1 e/Å$^3$, using the visualization software VESTA [28].

Figure 4(a) shows the 3D unit cell of BSZT with the (100) plane shaded for $x$ = 0. The positions of barium, titanium and oxygen atoms and the electron density distributions in their valence levels are explicitly and clearly seen from this figure. The qualitative analysis of

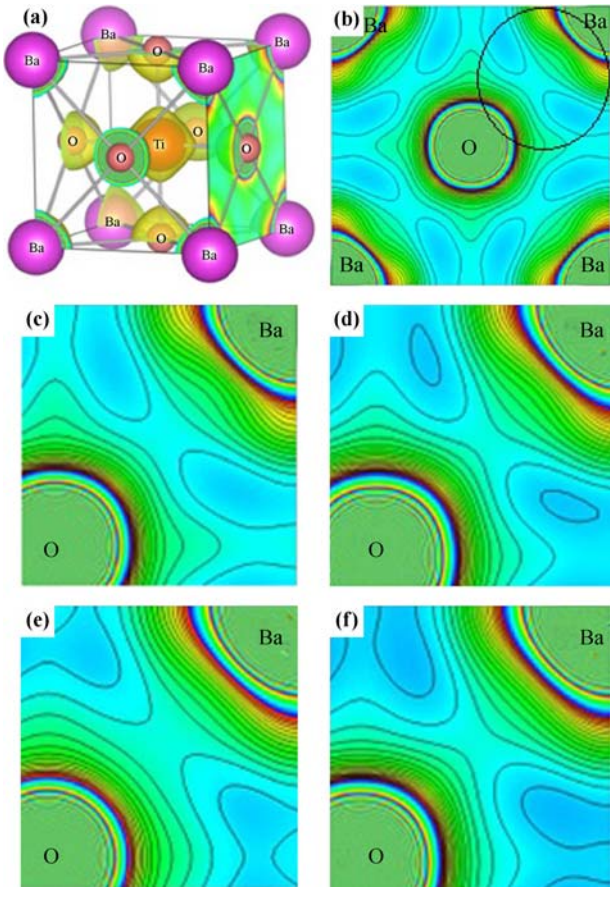


**Fig. 4** **(a)** 3D unit cell with the (100) plane shaded for $x = 0$. **(b)** 2D contour map on the (100) plane for $x = 0$. **(c)(d)(e)(f)** Enlarged views of Ba–O bonds for $x = 0$, 0.05, 0.07 and 0.14 on the (100) plane.

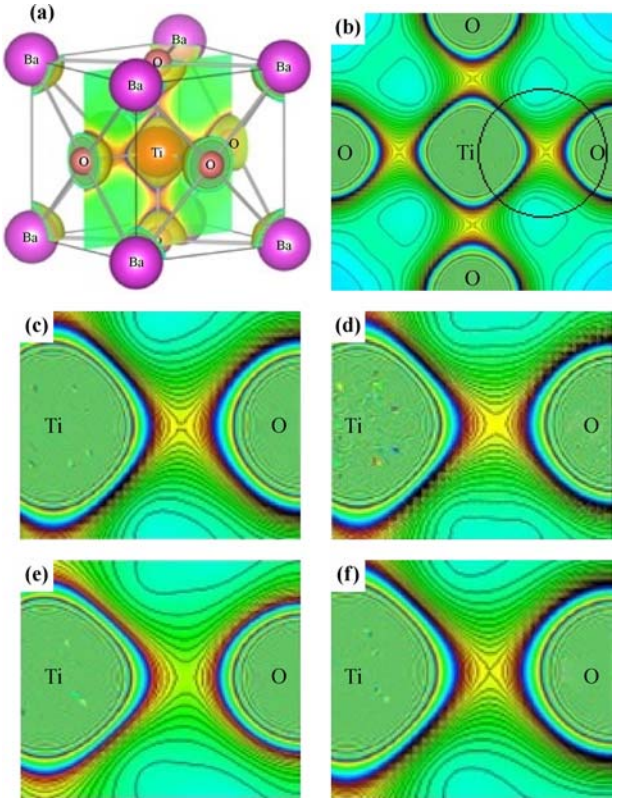


**Fig. 5** **(a)** 3D unit cell with the (200) plane shaded for $x = 0$. **(b)** 2D contour map on the (200) plane for $x = 0$. **(c)(d)(e)(f)** Enlarged views of Ti–O bonds for $x = 0$, 0.05, 0.07 and 0.14 on the (200) plane.

chemical bonding between barium and oxygen and between titanium and oxygen was done by plotting 2D charge density contour maps in the contour range of 0–1 e/Å$^3$ and with the contour interval of 0.04 e/Å$^3$, corresponding to two different crystallographic planes, (100) and (200).

Figure 4(b) shows the 2D contour map on the (100) plane for $x = 0$ and Figs. 4(c)–4(f) show the enlarged sections of Ba – O bond for different Sr concentrations $x = 0$, 0.05, 0.07 and 0.14 respectively. The contour lines around the Ba and O atoms clearly show that, there is no charge linkage between the Ba and O atoms. This clearly evidences the ionic nature of Ba – O bond. Figure 5(a) shows the 3D unit cell of BSZT with the (200) plane shaded for $x = 0$. Figure 5(b) shows the 2D contour map on the (200) plane for $x = 0$ and Figs. 5(c)–5(f) show the enlarged sections of Ti – O bond for different Sr concentrations $x = 0$, 0.05, 0.07 and 0.14 respectively. The overlapping of charge density distributions along the bond path of Ti and O evidenced the covalent nature of Ti – O bond.

To analyze the strength and nature of bonding quantitatively, 1D electron density profiles for Ba – O bond in the (100) plane and Ti – O bond in the (200) plane are drawn for all the compositions and analyzed. Figures 6 and 7 show the 1D line profiles of Ba – O and Ti – O bonds, respectively. The bond lengths and the electron density values at the bond critical points (BCP) of Ba – O and Ti – O bonds in the BSZT ceramic with different Sr doping levels are given in Table 2. The length of Ba – O bond for $x = 0$ is 2.8506 Å. The bond length is shortened from 2.8466 to 2.8323 Å with the increasing incorporation of Sr content. The length of Ti – O bond for $x = 0$ is 2.0157 Å. The bond length is shortened from 2.0128 to 2.0027 Å with the increasing incorporation of Sr content in accordant with the XRD results. For $x = 0$, the electron density value at the bond critical point of Ba – O bond is 0.2787 e/Å$^3$. For the Sr-doped compositions, the electron density values are slightly increasing. The low electron density values confirm the ionic nature of Ba – O bond. In the case of Ti – O bond, the electron density value at the bond critical

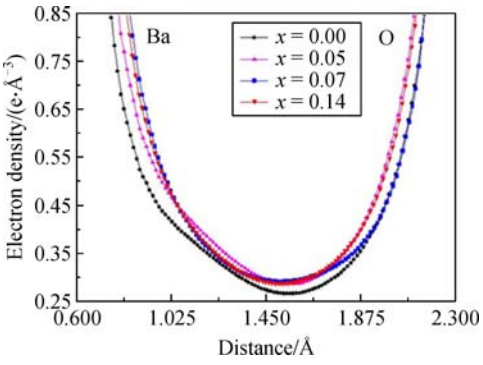


**Fig. 6** 1D electron density profiles along Ba and O atoms in$Ba_{1-x}Sr_xZr_{0.1}Ti_{0.9}O_3$ with $x$ = 0, 0.05, 0.07 and 0.14.

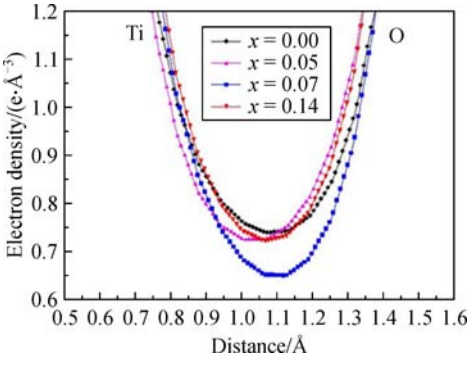


**Fig. 7** 1D electron density profiles along Ti and O atoms in $Ba_{1-x}Sr_xZr_{0.1}Ti_{0.9}O_3$ with $x$ = 0, 0.05, 0.07 and 0.14.

**Table 2** Bond lengths and electron density values at bond critical point (BCP) for Ba–O and Ti–O bonds for $Ba_{1-x}Sr_xZr_{0.1}Ti_{0.9}O_3$ with $x$ = 0, 0.05, 0.07 and 0.14

| Sample | Bond length /Å | | Electron density at BCP /(e·Å$^{-3}$) | |
|---|---|---|---|---|
| | Ba–O | Ti–O | Ba–O | Ti–O |
| $x$ = 0.00 | 2.8506 | 2.0157 | 0.2787 | 0.7615 |
| $x$ = 0.05 | 2.8466 | 2.0128 | 0.3022 | 0.7260 |
| $x$ = 0.07 | 2.8370 | 2.0061 | 0.2969 | 0.6801 |
| $x$ = 0.14 | 2.8323 | 2.0027 | 0.2943 | 0.7412 |

point for $x$ = 0 composition is 0.7615 e/Å$^3$ and for Sr-doped compositions shows the reduction in the electron density values. The electron density values confirm that, the nature of Ti–O bond is less ionic and partially covalent.

### 3.4 SEM/EDS measurements

The microstructural and the surface morphological studies of the prepared ceramic samples have been carried out by SEM. The SEM images of BSZT for various doping levels corresponding to ×10 000 magnification are given in Fig. 8. Particles with well defined grain boundaries are seen from the SEM images which show that, the simultaneous

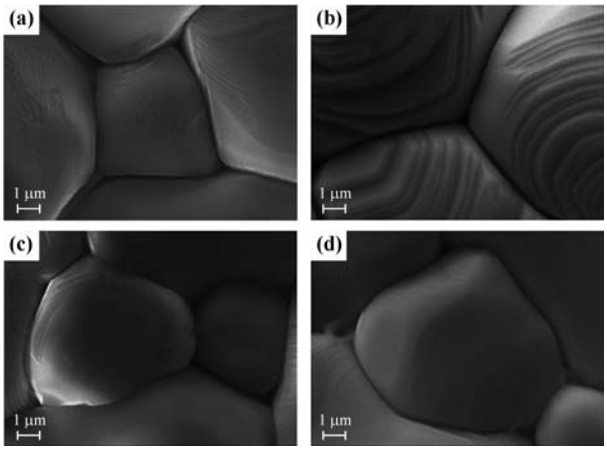


**Fig. 8** SEM images for $Ba_{1-x}Sr_xZr_{0.1}Ti_{0.9}O_3$: **(a)** $x$ = 0; **(b)** $x$ = 0.05; **(c)** $x$ = 0.07; **(d)** $x$ = 0.14.

substitution of Sr and Zr into the $BaTiO_3$ lattice promotes good grain growth. The qualitative analysis of the prepared BSZT ceramics has been carried out by analyzing the EDS spectra, which are depicted in Fig. 9. The existence of characteristic peaks corresponding to the main constituent elements of Ba, Ti, Zr, Sr and O is seen in the figures. No signature of any impurity peaks has been detected in the EDS spectra in all the compositional range. This clearly ensures the phase purity of the prepared samples similar to XRD patterns.

### 3.5 UV-visible analysis

The optical band gap values ($E_g$) for the synthesized BSZT samples have been evaluated by the method which was formulated by Wood and Tauc [29]. We have calculated the optical band gap of BSZT from the graph drawn by taking energy ($h\nu$) in $X$-axis and $(\alpha h\nu)^2$ in $Y$-axis which is shown in Fig. 10.

Then, by extrapolating the tangent from the linear portion of the curve to meet the $X$-axis at $(\alpha h\nu)^2 = 0$ gives the optical energy band gap value. Optical band gap values evaluated for various compositions of the BSZT systems are listed in Table 3. It is seen that the band gap values are decreasing with the incorporation of the Sr content which shows the slight reduction in the insulating property of the prepared systems.

## 4 Conclusions

The effects of Sr doping on the $Ba_{1-x}Sr_xZr_{0.1}Ti_{0.9}O_3$ crystal structure have been investigated by characterizing the prepared samples using PXRD, UV-visible spectro-

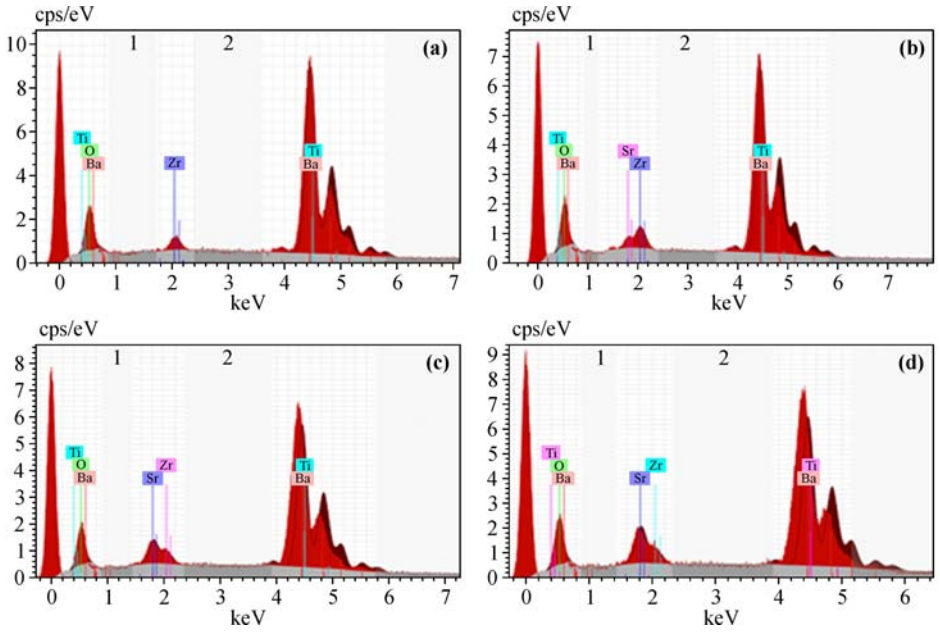


**Fig. 9** EDS spectra for $Ba_{1-x}Sr_xZr_{0.1}Ti_{0.9}O_3$: **(a)** $x = 0$; **(b)** $x = 0.05$; **(c)** $x = 0.07$; **(d)** $x = 0.14$.

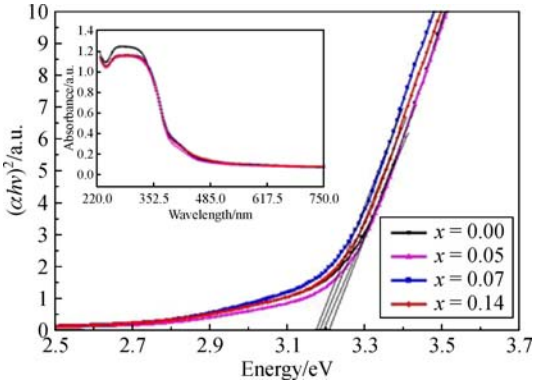


**Fig. 10** UV-visible plots for $Ba_{1-x}Sr_xZr_{0.1}Ti_{0.9}O_3$ with $x = 0$, 0.05, 0.07 and 0.14, the inset showing the UV-vis absorption spectra.

**Table 3** UV-visible parameters for $Ba_{1-x}Sr_xZr_{0.1}Ti_{0.9}O_3$ with $x = 0$, 0.05, 0.07 and 0.14

| Sample | Parameters | | |
|---|---|---|---|
| | Wavelength /nm | Absorbance /a.u. | Band gap energy /eV |
| $x = 0.00$ | 281 | 1.238 | 3.208 |
| $x = 0.05$ | 282 | 1.141 | 3.193 |
| $x = 0.07$ | 290 | 1.156 | 3.174 |
| $x = 0.14$ | 289 | 1.154 | 3.183 |

photometry, SEM and EDS. Powder X-ray data and powder profile refinement confirms that all the synthesized samples have been well crystallized in cubic perovskite structure with single phase. Electron density re-distribution and bonding interactions between Ba – O and Ti – O of the BSZT systems are precisely analyzed by the MEM. The predominant ionic nature between Ba and O ions and the covalent nature between Ti and O ions are revealed from charge density calculations. Optical band gap values are evaluated for the prepared samples from UV-visible absorption spectra. Formation of particles with well defined grain boundaries are visualized from SEM images. The phase purity of the prepared samples is further confirmed by EDS spectral analysis.

**Acknowledgements** The authors gratefully acknowledge the authorities of "The Madura College, Madurai-11" for providing lab facilities, continuous support and encouragement to carry out the research work successfully. One of the authors (J.M.) is thankful to the Management of NMSSVN College, Nagamalai, Madurai-19 and UGC for the Faculty Development Programme of XII plan, the period in which this effective work was carried out.

## References

[1] Rani R, Singh S, Juneja J K, et al. Dielectric properties of Zr substituted BST ceramics. Ceramics International, 2011, 37(8): 3755–3758

[2] Buscaglia M T, Buscaglia V, Viviani M, et al. Influence of foreign ions on the crystal structure of $BaTiO_3$. Journal of the European Ceramic Society, 2000, 20(12): 1997–2007

[3] Nanakorn N, Jalupoom P, Vaneesorn N, et al. Dielectric and ferroelectric properties of $Ba(Zr_xTi_{1-x})O_3$ ceramics. Ceramics International, 2008, 34(4): 779–782

[4] Wu T B, Wu C M, Chen M L. High insulative barium zirconate–titanate thin films prepared by rf magnetron sputtering for dynamic

random access memory applications. Applied Physics Letters, 1996, 69(18): 2659–2661

[5] Dixit A, Majumder S B, Katiyar R S, et al. Relaxor behavior in sol–gel derived $BaZr_{0.40}Ti_{0.60}O_3$. Applied Physics Letters, 2003, 82(16): 2679–2681

[6] Swartz S L. Topics in electronic ceramics. IEEE Transactions on Electrical Insulation, 1990, 25(5): 935–987

[7] Cavalcante L S, Sczancoski J C, De Vicente F S, et al. Microstructure, dielectric properties and optical band gap control on the photoluminescence behavior of $Ba[Zr_{0.25}Ti_{0.75}]O_3$ thin films. Journal of Sol-Gel Science and Technology, 2009, 49(1): 35–46

[8] Brankovic G, Brankovic Z, Goes M S, et al. Barium strontium titanate powders prepared by spray pyrolysis. Materials Science and Engineering B, 2005, 122(2): 140–144

[9] Caruntu G, Rarig R Jr, Dumitru I, et al. Annealing effects on the crystallite size and dielectric properties of ultra fine $Ba_{1-x}Sr_xTiO_3$ $(0<x<1)$ powders synthesized through an oxalate-complex precursor. Journal of Materials Chemistry, 2006, 16(8): 752–758

[10] Nedelcu L, Ioachim A, Toacsan M, et al. Synthesis and dielectric characterization of $Ba_{0.6}Sr_{0.4}TiO_3$ ferroelectric ceramics. Thin Solid Films, 2011, 519(17): 5811–5815

[11] Chan N Y, Choy S H, Wang D Y, et al. High dielectric tunability of ferroelectric $(Ba_{1-x},Sr_x)(Zr_{0.1},Ti_{0.9})O_3$ ceramics. Journal of Materials Science Materials in Electronics, 2014, 25(6): 2589–2594

[12] Kumar M, Garg A, Kumar R, et al. Structural, dielectric and ferroelectric study of $Ba_{0.9}Sr_{0.1}Zr_xTi_{1-x}O_3$ ceramics prepared by the sol–gel method. Physica B: Condensed Matter, 2008, 403(10–11): 1819–1823

[13] Bhaskar Reddy S, Prasad Rao K, Ramachandra Rao M S. Structural and dielectric characterization of Sr substituted Ba(Zr, Ti)$O_3$ based functional materials. Applied Physics A: Materials Science & Processing, 2007, 89(4): 1011–1015

[14] Bhaskar Reddy S, Prasad Rao K, Ramachandra Rao M S. Effect of La substitution on the structural and dielectric properties of $BaZr_{0.1}Ti_{0.9}O_3$ ceramics. Journal of Alloys and Compounds, 2009, 481(1–2): 692–696

[15] Jain A, Saroha R, Pastor M, et al. Effect of sintering duration on structural and electrical properties of $Ba_{0.9}Sr_{0.1}Ti_{0.96}Zr_{0.04}O_3$ solid solution. Current Applied Physics, 2016, 16(8): 859–866

[16] Wang X, Huang R, Zhao Y, et al. Dielectric and tunable properties of Zr doped BST ceramics prepared by spark plasma sintering. Journal of Alloys and Compounds, 2012, 533(1): 25–28

[17] Tawade C M, Madolappa S, Sharanappa N, et al. Microstructural and electrical study of $(Ba_{0.6}Sr_{0.4})(Zr_{1-x}Ti_x)O_3$ ceramics. IJRET, 2013, 2(8): 184–187

[18] Deng X Y, Wang X H, Li D J, et al. Electronic structure of nanograin barium titanate ceramics. Frontiers of Materials Science, 2007, 1(3): 316–318

[19] Saravanan R. Practical application of maximum entropy method in electron density and bonding studies. Physica Scripta, 2009, 79 (4): 048303 (8 pages)

[20] Rietveld H M. A profile refinement method for nuclear and magnetic structures. Journal of Applied Crystallography, 1969, 2 (2): 65–71

[21] Collins D M. Electron density images from imperfect data by iterative entropy maximization. Nature, 1982, 298(5869): 49–51

[22] Shannon R D. Revised effective ionic radii and systematic studies of interatomic distances in halides and chalcogenides. Acta Crystallographica, 1976, 32(5): 751–767

[23] Petricek V, Dusek M, Palatinus L. The crystallographic computing system JANA 2006: General features. Zeitschrift fur Kristallographie, 2014, 229(5): 345–352

[24] Wyckoff R W G. Crystal Structures, Vol. 2. London: Inter-space Publishers, 1963

[25] Thongtha A, Angsukased K, Riyamongkol N, et al. Preparation of $(Ba_{1-x}Sr_x)(Zr_xTi_{1-x})O_3$ ceramics via the solid state reaction method. Ferroelectrics, 2010, 403(1): 68–75

[26] Saravanan R. GRAIN software (personal communication)

[27] Izumi F, Dilanien R A. Recent Research Developments in Physics, Part II, Vol. 3. Trivandrum, India: Transworld Research Network, 2002

[28] Momma K, Izumi F. VESTA: a three-dimensional visualization system for electronic and structural analysis. Journal of Applied Crystallography, 2008, 41(3): 653–658

[29] Tauc J, Grigorovici R, Vancu Y. Optical properties and electronic structure of amorphous germanium. Physica Status Solidi B, 1966, 15(2): 627–637